CORA Cork Open Research Archive
Cartlann Taighde Oscailte Chorcaí

Title	Nonstationary signal decomposition using quadratic time–frequency distributions
Authors	O'Toole, J. M.;Stevenson, N. J.
Publication date	2025-07-12
Original Citation	O'Toole, J. M. and Stevenson, N. J. (2025) 'Nonstationary signal decomposition using quadratic time–frequency distributions', Signal Processing, 238, 110095 (11pp). https://doi.org/10.1016/j.sigpro.2025.110095
Type of publication	Article (peer reviewed)
Link to publisher's version	10.1016/j.sigpro.2025.110095
Rights	© 2025, the Author(s). Published by Elsevier B.V. This is an open access article under the CC BY license (http://creativecommons.org/licenses/by/4.0/). - https://creativecommons.org/licenses/by/4.0/
Download date	2026-11-04 11:07:27
Item downloaded from	https://hdl.handle.net/10468/17719



UCC
University College Cork, Ireland
Coláiste na hOllscoile Corcaigh

Signal Processing 238 (2026) 110095



Contents lists available at ScienceDirect

Signal Processing

journal homepage: www.elsevier.com/locate/sigpro



Nonstationary signal decomposition using quadratic time–frequency distributions

J.M. O'Toole [a,*], N.J. Stevenson [b]

[a] INFANT Research Centre, University College Cork, Cork, Ireland
[b] Brain Modelling Group, QIMR Berghofer Medical Research Institute, Brisbane, QLD, Australia

ARTICLE INFO

Dataset link: https://github.com/otoolej/tfd_decomp/

Keywords:
Signal decomposition
Quadratic time–frequency distributions
Time-varying filtering
Cross-time–frequency distributions
Signal modelling

ABSTRACT

Extracting and isolating individual components of a multi-component signal is an important but challenging task in signal processing. Signal components can be buried in noise, time-limited without temporal overlap, and can have minimal separation in the frequency domain. This work presents two methods for decomposing multi-component signals that overcome the limitations of separating signal energy, jointly, in both time and frequency domains. These methods use established peak-tracking algorithms to extract instantaneous frequency (IF) laws from contiguous regions of local-energy concentrations in a quadratic time–frequency distribution (TFD). The novelty of this work is in the methods that convert these IF laws into signal components using either (1) time-varying filter banks or (2) sinusoidal model fitting with cross-TFD phase corrections. We validate these methods using simulated and real-world signals and compare their performance against existing techniques such as the time-varying empirical mode decomposition, variational mode decomposition, and synchrosqueezed transforms. The proposed methods achieve superior efficacy for decomposition over a range of nonstationary signals, do not require *a priori* knowledge, such as centre frequencies or component number, and perform well in the presence of noise.

1. Introduction

Decomposing a signal into a series of components is an important task within the field of signal processing. Decomposition provides the signal analyst with opportunities to highlight signal components that are relevant and information rich as well as opportunities to discard artefactual or irrelevant signal components. This process of obtaining key signal components has many applications across a wide range of fields, such as speech and image processing [1,2], communications [3], biomedical engineering [4], and power systems [5].

Signal decomposition extracts J components from a signal of N samples in duration. Two of the more successful methods of signal decomposition are the discrete-time Fourier transform and discrete wavelet decomposition [6,7]. These methods are, to a degree, based on projections of a signal onto a set of basis functions and show excellent decomposition performance across a wide variety of signal processing problems. In these cases, $J = N$ with desirable decomposition properties such as high computational speed and complete signal representation, i.e. decomposition without a residual. It is possible to have $J \gg N$ when using methods with basis functions that are over-complete such as atomic decomposition [8], but a more interesting case with potentially greater utility is the under-determined problem where $J \ll N$. Here, several *a priori* assumptions about the type of signal under analysis guide the structure of the decomposition algorithm with the aim of extracting a minimum number of components that represent the maximum amount of information on the underlying signal emitting process. In this paper, we develop methods to decompose a particular class of nonstationary multi-component signals where $J \ll N$.

Nonstationary signals complicate the interpretation of traditional methods reliant on stationary basis functions as the number of basis functions required to represent the signal is excessively large when the frequency content varies over time. Techniques such as the empirical mode decomposition (EMD) have been developed to reduce the number of components extracted from nonstationary multi-component signals [9] with the aim of simplifying the interpretation of decomposed signal components. This popular method has been widely applied to a range of problems and is capable of extracting signal components, or intrinsic mode functions (IMFs), with time-varying frequency content as well as preserving signal components with multiple harmonics that are typically generated by nonlinear systems when driven by simple forcing functions. Limitations of EMD, such as the propensity to combine distinct signal components into a single IMF [10], have motivated the development of alternatives like ensemble EMD and time-varying

* Corresponding author.
E-mail addresses: jotoole@ucc.ie (J.M. O'Toole), Nathan.Stevenson@qimrberghofer.edu.au (N.J. Stevenson).

https://doi.org/10.1016/j.sigpro.2025.110095
Received 31 December 2024; Received in revised form 15 March 2025; Accepted 7 May 2025
Available online 3 July 2025
0165-1684/© 2025 The Authors. Published by Elsevier B.V. This is an open access article under the CC BY license (http://creativecommons.org/licenses/by/4.0/).

EMD (TV-EMD) [11–13]; mode decomposition remains an active area of research [14].

Another popular alternative to EMD is variational mode decomposition (VMD) [15], an iterative method that minimizes the bandwidth of each component in the frequency domain. VMD has proven effective in separating signal components with overlapping frequency content and has been applied to a wide range of signal processing problems [15]. Like EMD, VMD has inspired several variants [15,16], most notably variational nonlinear chirp mode decomposition (VNCMD), which is specifically designed to decompose signals with time-varying frequency content. VMD methods, however, are sensitive to the *a priori* selection of parameters, such as the number of components and the approximate centre frequency of each component—information that may not be readily available with nonstationary multi-component signals.

An alternative to the methods of mode decomposition is an approach that identifies components directly from the joint time–frequency distribution (TFD) of a signal. These components are defined using their instantaneous frequency (IF) laws which are loosely defined as contiguous areas of similar energy in the time–frequency plane. IF laws, and therefore components, can be estimated directly from the TFD and the signal components reconstructed under the assumption that over a short-time analysis window, the derivative of the IF with respect to time is close to zero. TFDs which preserve phase information, such as the short-time Fourier transform (STFT) or the continuous wavelet transform, permit direct inversion from the time–frequency domain to the time domain. These TFDs, however, have limited time–frequency resolution and require nearby signal energy to be focused around each component to sharpen the IF laws in the distribution; a process known as reassignment. After reassignment, signal components identified using the IF law are reconstructed using the synchrosqueeze method [17–19].

Quadratic TFDs (QTFDs) offer increased time–frequency resolution compared to the STFT or wavelet distributions [20–22]. Phase information, however, is lost in QTFDs and inversion to extract individual components in the time domain is not possible. We propose two methods that bypass this limitation. The first method passes the signal through an array of linear time-invariant filters with parameters derived from the estimated IF law to separate signal components. The second method uses sinusoidal model fitting with the IF laws and instantaneous amplitude estimated from the QTFD and then refines the model fit using the instantaneous phase of a complex-valued cross-TFD (XTFD) between the signal and initial fit. We show that both methods have a high level of efficacy when decomposing nonstationary multi-component signals, particularly in the case of signals with components that are non-adjacent or disjoint in the joint time–frequency domain.

2. Background

2.1. Mode decomposition

The EMD decomposes a signal by iteratively removing the short-time mean of the signal envelope from a residual, starting with the original signal [9]. This local mean is estimated as the average of an upper and lower limit of a signal, defined by fitting splines to all local maxima and minima. The local mean is subtracted from the current residual, and the process—known as *sifting*—is repeated on the resulting residual until the difference between successive sifted signals is minimized, or the number of extrema (maxima and minima) approaches equality. Sifting ensures that the resultant IMF is amenable to calculating meaningful amplitude-modulated (AM) and frequency-modulated (FM) components of a typical multi-component signal model, such as

$$x(t) = \sum_{j=1}^{L} a_j(t) \sin\left(2\pi\theta_j(t) + \phi_j\right) \tag{1}$$

where $a_j(t)$ is the AM and $\sin(2\pi\theta_j(t) + \phi_j)$ the FM term of the j^{th} signal component, and where the AM mean frequency is considerably lower than the FM mean frequency. The remaining residual after sifting defines an intrinsic mode function (IMF).

The EMD is a data-driven technique without analytic representation although several studies have revealed interesting properties of the EMD. Notably, components (IMFs) tend to be separated into logarithmic frequency scales, when signal energy is sufficiently present to ensure signal extrema across the frequency scale. Also, continuity in time is enforced which can result in the merging of potential disparate signal components together—the so-called *riding waves* problem [10,23]. An advantage of the EMD is that it merges harmonics into a single component, provided the harmonics do not generate additional extrema. This property is particularly useful when analysing signals from nonlinear systems with time-varying frequency content.

Variational mode decomposition (VMD) has emerged as a popular alternative to the EMD and its variants. VMD is an iterative optimization method that extracts components, assumed to be compact in the frequency domain, by minimizing the bandwidth of each component. Unlike the EMD, VMD is a non-recursive method that optimizes all components simultaneously. It also has a rigorous mathematical framework, in contrast to EMD's heuristic approach [15]. However, the method does require the number of components and the approximate centre frequency of each component as input parameters, which in many instances may not be known or easily estimated.

2.2. Quadratic time–frequency distributions

Time–frequency signal analysis provides a suitable framework for analysing nonstationary signals. By transforming a time-domain signal into a joint time–frequency representation, the signal's characteristics can be simultaneously tracked in both time and frequency. This transformation enables the application of various time–frequency analysis techniques to effectively extract and process information from the signal [22].

Quadratic time–frequency distributions (QTFDs) are high-resolution representations with robust theoretical foundations [20–22]. This class of distributions has become a widely adopted and popular choice for time–frequency analysis. A QTFD, for signal $x(t)$ of infinite duration, is defined as

$$\rho_z(t,f) = W_z(t,f) \underset{(t,f)}{**} \phi(t,f) \tag{2}$$

where $W_z(t,f)$ is the Wigner–Ville distribution (WVD) of the signal $z(t)$, $\phi(t,f)$ is known as the time–frequency kernel function, and $**$ denotes the convolution operator, which is applied across time (t) and frequency (f) [22]. The WVD is defined as the Fourier transform of the time-varying auto-correlation function of the signal $z(t)$,

$$W_z(t,f) = \int_{-\infty}^{\infty} z(t+\tfrac{\tau}{2}) z^*(t-\tfrac{\tau}{2}) \mathrm{e}^{-\mathrm{j}2\pi f\tau} \mathrm{d}\tau \tag{3}$$

where $z^*(t)$ is the complex conjugate of $z(t)$. The complex signal $z(t)$ is derived from the real-valued signal $x(t)$ to form the analytic signal $z(t) = x(t) + \mathrm{j}\mathcal{H}\{x(t)\}$, where j is the imaginary unit and $\mathcal{H}$ is the Hilbert transform [22]. The analytic signal has zero energy at negative frequencies which ensures that the distribution maintains important properties and avoids aliasing in the discrete case [21,24].

The WVD can provide a compact time–frequency representation of signal energy. For example, the WVD of a complex sinusoid and impulse signal are both represented as delta functions in the time–frequency domain as [21]

$$\begin{aligned} z(t) &= \mathrm{e}^{j2\pi f_0}, & W_z(t,f) &= \delta(f-f_0) \\ z(t) &= \delta(t-t_0), & W_z(t,f) &= \delta(t-t_0). \end{aligned} \tag{4}$$

For a linear frequency modulated (LFM) signal, the WVD is a time-varying delta function along the instantaneous frequency of signal,

$$z(t) = \mathrm{e}^{j2\pi(tf_0+\beta t^2/2)}, \quad W_z(t,f) = \delta(f-f_0-\beta t). \tag{5}$$

Although the WVD has many desirable mathematical properties, such as satistying marginal constraints, it has some limitations, particularly for multicompnent signals. Because of the quadratic nature of the WVD, the superposition of two signals results in the following:

$$W_z(t,f) = W_{z_1+z_2}(t,f) = W_{z_1}(t,f) + W_{z_2}(t,f) + 2\mathrm{Re}\left\{W_{z_1 z_2}(t,f)\right\}. \quad (6)$$

for $z(t) = z_1(t) + z_2(t)$, where $\mathrm{Re}\left\{W_{z_1 z_2}(t,f)\right\}$ is the real part of the complex-valued distribution

$$W_{z_1 z_2}(t,f) = \int_{-\infty}^{\infty} z_1(t+\tfrac{\tau}{2}) z_2^*(t-\tfrac{\tau}{2}) \mathrm{e}^{-\mathrm{j}2\pi f\tau}\,\mathrm{d}\tau \quad (7)$$

This cross-WVD $W_{z_1 z_2}(t,f)$ consists of cross-terms components which introduces interference in the WVD $W_{z_1+z_2}(t,f)$, therefore making it difficult to extract information. Hence the addition of the kernel function $\phi(t,f)$ in (2) for QTFDs—the kernel is designed to suppress these cross-terms by smoothing the distribution in the time–frequency domain [22]. The class of QTFDs is therefore defined by different kernels $\phi(t,f)$ which act as time–frequency filters to remove unwanted cross-terms.

2.3. Estimating instantaneous frequency

For a monocomponent signal, the instantaneous frequency (IF) of a signal is defined as the derivative of the instantaneous phase of the signal [22]; that is, for a signal $z(t) = a(t)\mathrm{e}^{j\theta(t)}$, the IF is defined as

$$f(t) = \frac{1}{2\pi}\frac{\mathrm{d}\theta(t)}{\mathrm{d}t}. \quad (8)$$

For the sinusoidal and LFM signals in (4) and (5), the IFs are f_0 and $f_0 + \beta t$, respectively. The IFs can also be estimated from the peak of the WVD, which for the LFM example would be

$$\hat{f}(t) = \arg\max_f W_z(t,f) = f_0 + \beta t. \quad (9)$$

Although the QTFD convolution in (2) introduces smoothing, the location of the peaks do not change and therefore the IF can be estimated by tracking the peak of the distribution [22]. This peak-tracking method for IF estimation is prevalent in various time–frequency and time-scale methods [17,19,25–27]. There are different techniques for peak tracking, but the most common and straightforward approach is to estimate the local maxima of the QTFD and track the peak over time. For the discrete QTFD, local peaks are estimated across a frequency vector for each time instance (time-slice). Then an algorithm is used to link the peaks across time to estimate a track to represent the IF laws. The assumption is that the IFs are continuous and slow-varying over time.

There are a number of challenges with peak-tracking. First, the number of detected peaks can vary from time-slice to time-slice, with the disappearance of peaks and the appearance of new peaks. Second, as the IF changes over time, a simple ordering of the peaks per time-slice may not be sufficient to track the peaks across time. Third, some peaks may belong to sidelobes or cross-terms between components, and therefore should not be included in the tracking process.

The following process describes an established algorithm, proposed by McAulay and Quatieri [25], for addressing these challenges. (As we are dealing with discrete signals and distributions, we switch notation; for signal x for example, from $x(t)$ to $x[n]$.) The algorithm first estimates all local peaks per time-slice. Then, it sorts and links the peaks from time-slice n to $n+1$ using the following process, where p_n^i represents the i^{th} peak at time-slice n:

- **Step 1:** determine if there are peaks p_{n+1}^i within an allowable frequency range (Δk); that is, if $p_{n+1}^i \in \left\{f_a[n] - \Delta k/2, f_a[n] + \Delta k/2\right\}$ where $f_a[n]$ is an existing track (see Fig. 1a for an example). If so, a tentative match is made and p_{n+1}^i is included in the track ($f_a[n+1] = p_{n+1}^i$). If not, the track $f_a[n]$ ends at n.
- **Step 2:** If another track $f_b[n]$ provides a better match to p_{n+1}^i, where $|p_{n+1}^i - f_b[n]| < |p_{n+1}^i - f_a[n]|$, then this track is updated to $f_b[n+1] = p_{n+1}^i$. (In the case of a tie, when $|p_{n+1}^i - f_b[n]| = |p_{n+1}^i - f_a[n]|$, p_{n+1}^i is matched to the higher frequency track $f_b[n+1]$; see Fig. 1b for an example.) If not, then the tentative match in Step 1 is confirmed and the track is updated to $f_a[n+1] = p_{n+1}^i$. If $f_a[n+1]$ did not match with p_{n+1}^i, then a peak at lower frequency p_{n+1}^{i+1} is considered for $f_a[n+1]$ (re-assessing the procedure from Step 1).
- **Step 3:** If peak at p_{n+1}^i has not been matched to an existing track, then a new track is created with $f_c[n+1] = p_{n+1}^i$.

This process is illustrated in Fig. 1 and described in more detail in Ref. [25]. An upper limit on the number of peaks per time-slice is enforced (peaks are ranked based on amplitude). Additional, after all tracks are created, a predefined parameter of minimum length is enforced to remove short-duration tracks. These two steps avoid including spurious tracks that are unlikely to represent real IF laws [22,25,28].

3. Methods

We define a discrete-time version of the multi-component nonstationary signal in (1) as the *sinusoidal model* as,

$$x[n] = \sum_{j=1}^{J} y_j[n] \quad (10)$$

$$y_j[n] = a_j[n]\sin\left(2\pi\theta_j[n] + \phi_j\right) \quad (11)$$

$$\theta_j[n] = \frac{1}{f_s}\sum_{m=0}^{n} f_j[m] \quad (12)$$

where n is discrete-time for $n = 0, 1, \ldots, N-1$ and f_s is the sampling frequency; to simplify notation we assume that $f_s = 1$ hereafter. For the j^{th} signal component, $a_j[n]$ is amplitude modulation, $\theta_j[n]$ is signal phase, and ϕ_j is the phase offset. Time-varying phase $\theta_j[n]$ is derived through the integration (cumulative sum) of the IF, $f_j[n]$. This AM/FM model of $y_f[n]$ is a common signal representation [22]. Although there are an infinite number of $\{a[n], \theta[n]\}$ combinations that will result in the same $x[n]$, there is a desired selection of $\{a[n], \theta[n]\}$ that constrains the frequency content of $a[n]$ to be considerably lower than $\sin\left(2\pi\theta_j[n]\right)$ [29]. The aim of signal decomposition methods are, therefore, to calculate $y_j[n]$ via estimates of $\{a[n], \theta[n]\}$.

Our approach to calculating $y_j[n]$ in (10) involves three steps.

1. Generate a QTFD, $\rho_{xx}[n,k]$. QTFDs provide a high-resolution estimate of the distribution of signal energy in a joint time–frequency domain. See example in Fig. 2a–b.
2. Identify signal component IF laws, $f_j[n]$, and therefore $\theta_j[n]$. Contiguous areas of similar energy above the noise floor in a QTFD are collected together to define a signal component. We use peak-tracking algorithms to estimate the number of signal components J and reconstruct their IF laws (described in Section 2.3 and illustrated in Fig. 2c).
3. Extract components $y_j[n]$ for $j = 1, 2, \ldots, J$. The two proposed methods are identical for step 1 and 2, but differ at this point. The first method uses time-varying filtering; the signal component $y_j[n]$ is generated by passing the signal through J filters defined for each discrete-time sample n (Fig. 2d). The second method constructs an approximation of the component using the sinusoidal model in (10) with the estimated IF laws $f_j[n]$ and instantaneous amplitude $a_j[n]$ as a basis and then refines this approximation by adjusting the instantaneous phase estimated from a XTFD (Fig. 2e).

We use a smoothed QTFD to form a representation of signal energy in the time–frequency domain. Rewriting the QTFD definition in (2) for the more general case of two discrete signals $x[n]$ and $y[n]$ as

$$\rho_{xy}[n,k] = \underset{m\to k}{\mathrm{DFT}}\left\{\underset{l\leftarrow n}{\mathrm{IDFT}}\left\{\underset{n\to l}{\mathrm{DFT}}\left\{x[n+m]y^*[n-m]\right\} H[l]g[m]\right\}\right\} \quad (13)$$

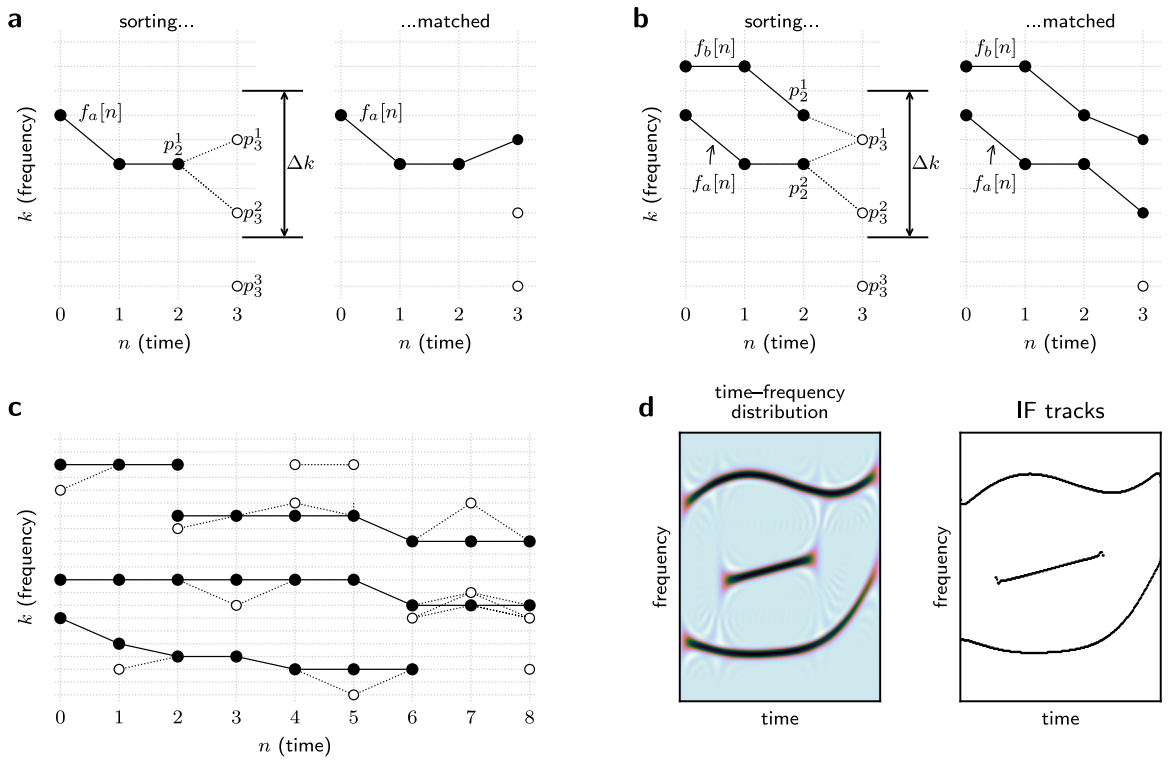


Fig. 1. Peak-tracking algorithm for estimating instantaneous frequency (IF) from a time–frequency distribution (TFD). Given a set of peaks p_n^i, for $i = 1, 2, \ldots, P_n$ at time n, the algorithm matches peaks to existing IF tracks, generates new tracks, or ends existing tracks. An example in (**a**) illustrates this matching process for time $n = 2$ to $n = 3$ for an existing IF track $f_a[n]$ and set of peaks $P_3 = 3$. Black lines represent the IF tracks and dotted lines represent potential matches; black dots (•) represent matched peaks and unfilled dots (∘) represent unmatched peaks. Only peaks within the predefined frequency range Δk are considered for matching. Another example in (**b**) of searching for candidate peaks with two IF tracks in consideration. IF $f_b[n+1]$ matches to peak p_3^1 and $f_a[n+1]$ matches to the lower frequency peak p_3^2. Example in (**c**) illustrates four IF tracks (black lines) and includes the potential matches (dotted lines) made during the sorting procedure. The peaks that are not matched to an IF, as illustrated by the unfilled dots (∘), are discarded. TFD in (**d**) of a signal with 3 components together with the estimated IF tracks using the peak-tracking algorithm.

where n is discrete-time, k is discrete-frequency, m is an additional variable of discrete-time (known as lag), l is an additional discrete-frequency variable (known as Doppler), DFT is the discrete Fourier transform and IDFT is the inverse DFT [30]. The separable kernel $H[l]g[m]$ is defined in the Doppler–lag $[l, m]$ domain and defines the smoothness of the QTFD. The signals under analysis, x and y, are analytic signals [24]. When $x = y$ the QTFD is generated; when $x \neq y$, the XTFD is generated. The kernel acts as smoothing window, spreading energy in both time and frequency domains. The window tends to be longer in the time direction under the assumption that continuity in time will exceed variation in the frequency domain; an assumption that aligns with our perceptions of signal components as defined in (10).

Signal components are derived from contiguous concentrations of energy within the QTFD [25]. These sequences of $[n, k]$ coordinates correspond to the IF law of each signal component in the QTFD. The peak-tracking algorithm describe in Section 2.3 is applied to the QTFD to find the IF tracks. To conform with our concept of slowly-varying continuous components with a significant extent in time, potential IF tracks that are too short or vary too rapidly in time are rejected. In this case, we set the minimum IF duration to $4\sqrt{N}$ and maximum rate of change (Δk in Fig. 1) to $\sqrt{N}/2$, assuming signal length N and a QTFD of size $N \times N$.

Once the QTFD is calculated and IF tracks extracted then signal components are reconstructed from the IF tracks using two independent methods. Code for both proposed decomposition methods is available at https://github.com/otoolej/tfd_decomp/.

3.1. Method 1: Time-varying filtering

The time-varying filter is implemented using finite-impulse response (FIR) filters [31] with specifications that vary at each discrete-time point n. The filter specification is defined by the IF laws extracted from the QTFD. The filter for the j^{th} component is defined as,

$$h_j[n,m] = \frac{w[m]}{\pi(m-\alpha)}\left[\sin(2\pi f_u[n](m-\alpha)) - \sin(2\pi f_l[n](m-\alpha))\right]$$
$$f_l[n] = \begin{cases} f_j[n] - B_1[n] & f_j[n] - B_1[n] > 0 \\ 0 & \text{otherwise} \end{cases} \tag{14}$$
$$f_u[n] = \begin{cases} f_j[n] + B_2[n] & f_j[n] + B_2[n] < 0.5 \\ 0.5 & \text{otherwise} \end{cases}$$

where M is the filter length (M is odd and $\alpha = (M-1)/2$), m and n are discrete-time, $f_j[n]$ is the discrete IF law of the j^{th} component, $B_1[n]$ and $B_2[n]$ are the bandwidth of the filter at time n and are defined as the midpoint between nearest components (if no component exists with lower or higher frequencies at n then B_1 and B_2, respectively, are undefined), normalized frequency limits are defined as $\{0, 0.5\}$, and $w[n]$ is a Hamming window of length M.

The use of variable filter bandwidths as defined by $\{B_1[n], B_2[n]\}$ ensures that the entire time–frequency plane is included in the decomposition resulting in a complete decomposition (i.e. zero residuals). A further caveat for completeness is that the IF laws completely span the temporal extent of the signal and type I FIR filters are used [7] as low, high and band pass filters are all used in the decomposition. In practice, we found $M = 2\left\lfloor\sqrt{N} + 1/2\right\rfloor - 1$ to be a useful filter length. The instantaneous filter bandwidths $\{B_1[n], B_2[n]\}$ can be tightened/reduced if a non-zero residual is desired for noise rejection. The complete procedure is detailed in Algorithm 1.

3.2. Method 2: Model fitting using a XTFD

The second method directly estimates the parameters of the multi-component nonstationarity sinusoidal model in (10). First, similar to

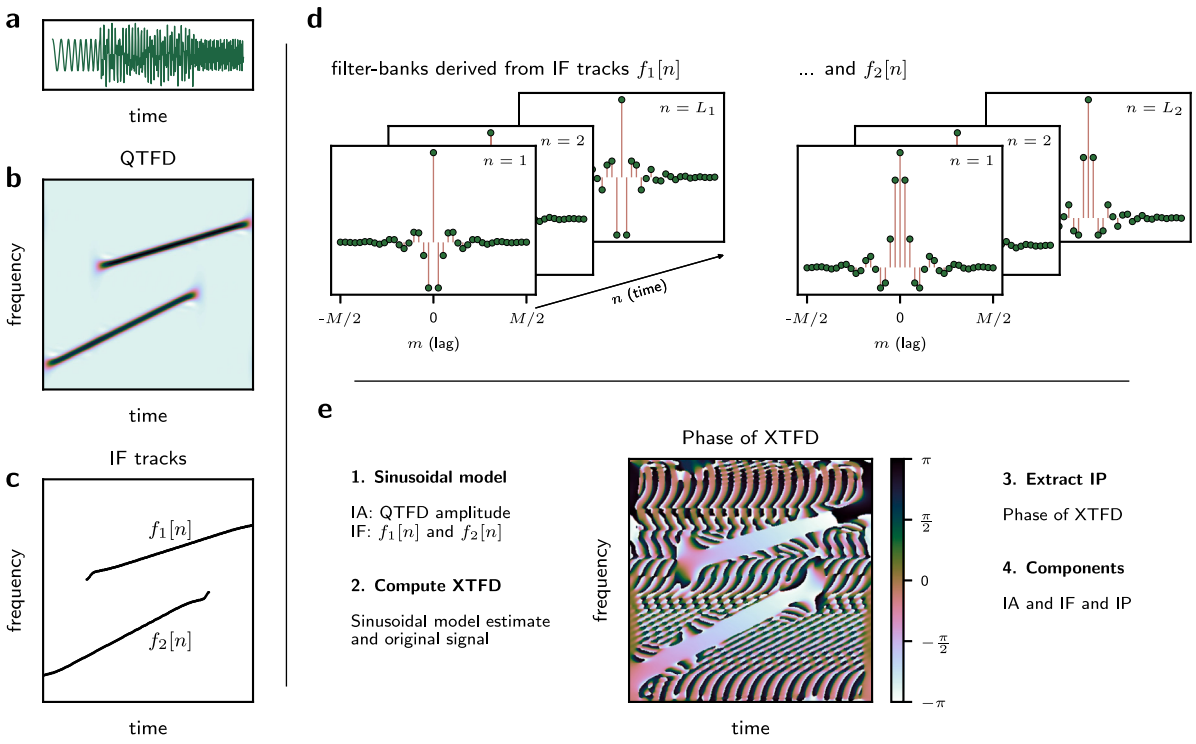


Fig. 2. Overview of the proposed signal decomposition methods. Signal in (**a**) is transformed to the time–frequency domain using a quadratic time–frequency distribution (QTFD) in (**b**) and the instantaneous frequency (IF) components are extracted as tracks in (**c**). Method 1 applies time-varying filtering to the signal; the series of time-varying impulse-response functions are presented in (**d**) for this example. Method 2, outlined in (**e**), generates a sinusoidal model of the signal using amplitude of the QTFD (instantaneous amplitude, IA) and the IF tracks. This is then used to generate a cross-TFD (XTFD). Instantaneous phase (IP) is extracted from the phase of the XTFD along the IF tracks. Each component is generated using the IA, IF, and IP terms.

Algorithm 1 TV Filtering Signal Decomposition

Input: signal $x[n]$ of length N
Output: J components $y_j[n]$
Parameters: TFD kernel parameters
1: Generate the TFD $\rho_{xx}[n,k]$ for signal $x[n]$
2: Calculate J IF laws $f_j[n]$ from $\rho_{xx}[n,k]$
3: Ensure IF tracks span the entire duration of the signal
4: **for** $j = 1, 2, \ldots, J$ **do**
5: Calculate time-varying filter cutoffs $\{f_l[n], f_u[n]\}$ defined in (14)
6: Generate time-varying windowed FIR filter with $\alpha = (M-1)/2$

$$h_j[n,m] = \frac{w[m]}{\pi(m-\alpha)}(\sin(2\pi f_u[n](m-\alpha)) - \sin(2\pi f_l[n](m-\alpha)))$$

7: **for** $n = 0, 1, \ldots, N-1$ **do**

$$y_j[n] = \sum_{m=-\alpha}^{\alpha} h_j[n,m]x[n-m]$$

8: **end for**
9: **end for**

the time-varying filter method, we estimate the IF laws $f_j[n]$ for each component using the QTFD. Next, we generate an initial estimate of the instantaneous amplitude $a_j[n]$ as the QTFD amplitude along the extracted IF law (step 4 in Algorithm 2). The method then generates an initial estimate of the signal $e[n]$, using $a_j[n]$ and $f_j[n]$ in the sinusoidal model

$$e[n] = \sum_{j=1}^{J} \sqrt{a_j[n]}\sin(2\pi \sum_{n=0}^{N-1} f_j[n]). \tag{15}$$

In practice, we found that there was a time-varying phase discrepancy between $e[n]$ and the signal $x[n]$. To correctly align the signal components in time, we estimate the instantaneous phase for each component using the XTFD $\rho_{xe}[n,k]$, generated between the signal $x[n]$ and the signal estimate $e[n]$. The XTFD is a complex-valued function and the instantaneous phase for the jth-component is estimated along the IF laws $f_j[n]$ as

$$\phi_j[n] = \angle\rho_{xe}[n, f_j[n]]. \tag{16}$$

In the TFD, the convolution of the lag kernel $g[m]$ smears the components in the frequency direction, thus expanding the bandwidth and reducing the amplitude. We do the following to correct for this process when estimating the instantaneous amplitude $a_j[n]$. First, we calculate the instantaneous bandwidth $b_j[n]$ for each component using the QTFD. The bandwidth is defined as the width of the component −3 dB from the time–frequency peak ($\rho_{xx}[n, f_j[n]]$ at n). We then scale $a_j[n]$ with a normalized-version of $b_j[n]$ to obtain

$$a_j[n] \leftarrow \frac{a_j[n]\, b_j[n]}{b_j[n_{\max}]} \quad \text{where} \quad n_{\max} = \arg\max_n a_j[n] \tag{17}$$

This process adjusts for the inherent time–frequency smoothing in the TFD and improves the estimate of $a_j[n]$.

The components are then generated using the sinusoidal model with instantaneous phase, as shown in (18). This method, which we refer to as the XTFD method, is based on generating components using the sinusoidal model from IF components identified in the TFD, and, therefore, does not necessarily process the entire time–frequency plane, providing an avenue for noise reduction or suppression.

Both decomposition methods rely on an appropriate time–frequency representation of the signal. We defined the smoothing window of our QTFD using two kernel parameters, length of the lag and Doppler windows in (13) which control the time–frequency resolution. The specific parameters used for each test signal are presented in Table S1

Algorithm 2 Cross Time–Frequency Distribution (XTFD) Signal Decomposition

Input: signal $x[n]$ of length N
Output: J components $y_j[n]$
Parameters: TFD kernel parameters

Generate the TFD $\rho_{xx}[n,k]$ for signal $x[n]$
Calculate J IF tracks $f_j[n]$ from $\rho_{xx}[n,k]$
for $j = 1, 2, \ldots, J$ **do**
    Calculate instantaneous amplitude: $a_j[n] = \rho_{xx}[n, f_j[n]]$
end for
Generate first estimate of the signal combining all components:

$$e[n] = \sum_{j=1}^{J} \sqrt{a_j[n]} \sin(2\pi \sum_{n=0}^{N-1} f_j[n])$$

Compute the XTFD $\rho_{xe}[n,k]$ between $x[n]$ and $e[n]$ using (13)
for $j = 1, 2, \ldots, J$ **do**
    Calculate instantaneous phase: $\phi_j[n] = \angle\rho_{xe}[n, f_j[n]]$
    Adjust instantaneous amplitude (see (17) details)

$$a_j[n] \leftarrow \frac{a_j[n]\, b_j[n]}{b_j[n_{\max}]}$$

    Generate component:

$$y_j[n] = \sqrt{a_j[n]} \sin(\phi_j[n] + 2\pi \sum_{n=0}^{N-1} f_j[n]) \tag{18}$$

end for

in the Supplementary Material. For the XTFD method for the first test signal, we over-sample the QTFD in the frequency domain to improve estimation of IF, instantaneous amplitude, and instantaneous phase. Oversampling is implemented using computationally efficient algorithms described elsewhere [30].

3.3. Test signals

We apply both methods of signal decomposition, as well as several existing methods, to a variety of simulated signals highlighting potential strengths and weaknesses. Firstly, the ability of the decomposition to extract stationary signal components with different frequencies is tested using a simple two-tone test. This is a common test signal for decomposition methods [13,32,33]. The two-tone test signal is defined as,

$$x[n] = y_1[n] + y_2[n] = \cos[2\pi n] + a\cos[2\pi k n]. \tag{19}$$

with signal length $N = 1,024$.

Secondly, the ability of the decomposition to extract signal components with different finite-time extents is tested using a windowed two-tone test signal described as,

$$\begin{aligned} y_1[n] &= w[n]\cos[2\pi n] \\ y_2[n] &= w[N-n]a\cos[2\pi k n] \end{aligned} \tag{20}$$

where window $w[n]$ is defined as

$$w[n] = \begin{cases} u[n] & \text{for } 0 \le n \le N/3 \\ 0 & \text{otherwise} \end{cases}$$

and $u[n]$ is a Tukey window with $\alpha = 0.2$. The window $w[n]$ provides a smooth transition to time-limit each component. For (19) and (20), a ranges from $0.01 \le a \le 100$ and frequency k is varied from $0.012 \le k \le 0.975$.

Thirdly, the ability of the decomposition to extract signal components from a real-world nonstationary and multi-component signal is tested using a recording of an echolocation pulse from a bat. This signal is commonly used for testing in time–frequency signal analysis [22].

Next, we test the ability of the decomposition method to extract signal components from a more complex, simulated multi-component nonlinear signal with three components: two nonlinear FM signals with slowly-varying and non-overlapping IF laws [34] and a time-limited linear FM signal, in the presence of fractional Gaussian noise with signal-to-noise ratios (SNRs) ranging from −4 to 10 dB. The QTFD of this signal is presented in Fig. 5b.

Finally, we examine the extracted signal components when the decomposition method is applied to white and fractional Gaussian noise. We use white Gaussian noise with zero mean and a standard deviation of one. We define fractional Gaussian noise as a stochastic signal with a $1/f^{2H-1}$ spectral response (setting $H = 0.2$). Both signals are $N = 128$ samples in duration.

3.4. Performance analysis

For the simulated two-tone signals, the error between the first estimated component ($c_1[n]$) from the signal decomposition and the simulated component ($y_1[n]$) was used to determine the decomposition efficacy over a range of amplitude and frequency ranges [13,32,33]. The relative error was defined as

$$e_{\text{rel}} = \frac{\left\| c_1[n] - y_1[n] \right\|_2}{\left\| y_2[n] \right\|_2} \tag{21}$$

where $\|\cdot\|_2$ represents the L^2 norm over the duration of the signal. In addition, we also include Pearson's correlation coefficient as an additional accuracy measure.

For the multi-component signal, we used the average relative error across all three components to define the efficacy of the decomposition, i.e.

$$e_{\text{rel}} = \frac{1}{3} \sum_{i=1}^{3} \frac{\left\| c_i[n] - y_i[n] \right\|_2}{\left\| y_i[n] \right\|_2} \tag{22}$$

where $c_i[n]$ is the extracted component and $y_i[n]$ is simulated component. This nonlinear signal is also used to perform an analysis of decomposition efficacy in the presence of noise.

For real signals, efficacy is judged subjectively against components defined by visual interpretation of the TFD. For example the bat echolocation signal shows three to four components in the time–frequency domain (see Fig. 4a) depending on the QTFD kernel and visualization process [19,22].

We also evaluate the compactness of the decomposition method by calculating the minimum number of extracted components M that represent 90% of the total signal energy. Number of components M is determined by summing the individual energy of each components until reaching at least 90% total signal energy. And lastly, we determine the computational speed for each method by evaluating 100 iterations of each test signal for each method. Simulations were performed using Matlab (version R2021a; The Mathworks, Natick, MA, USA) on a laptop computer with an Intel i7 processor (8 cores) and 16 GB of RAM.

We compare our proposed methods against several other methods, including empirical Fourier decomposition (EFD) [33], time-varying empirical mode decomposition (TV-EMD) [13], synchrosqueeze short-time Fourier transform (SSFT) [35], variational mode decomposition (VMD) [12], and variational nonlinear chirp mode decomposition (VNCMD) [15]. We made every effort to maximize the performance of these methods across different signal types by setting appropriate internal parameters. For the SSFT, we used the Matlab function `fsst()` to estimate the synchrosqueeze transform and `tfridge()` and `ifsst()` to estimate the time–frequency tracks and generate the components; for all other methods we used code supplied by the authors.

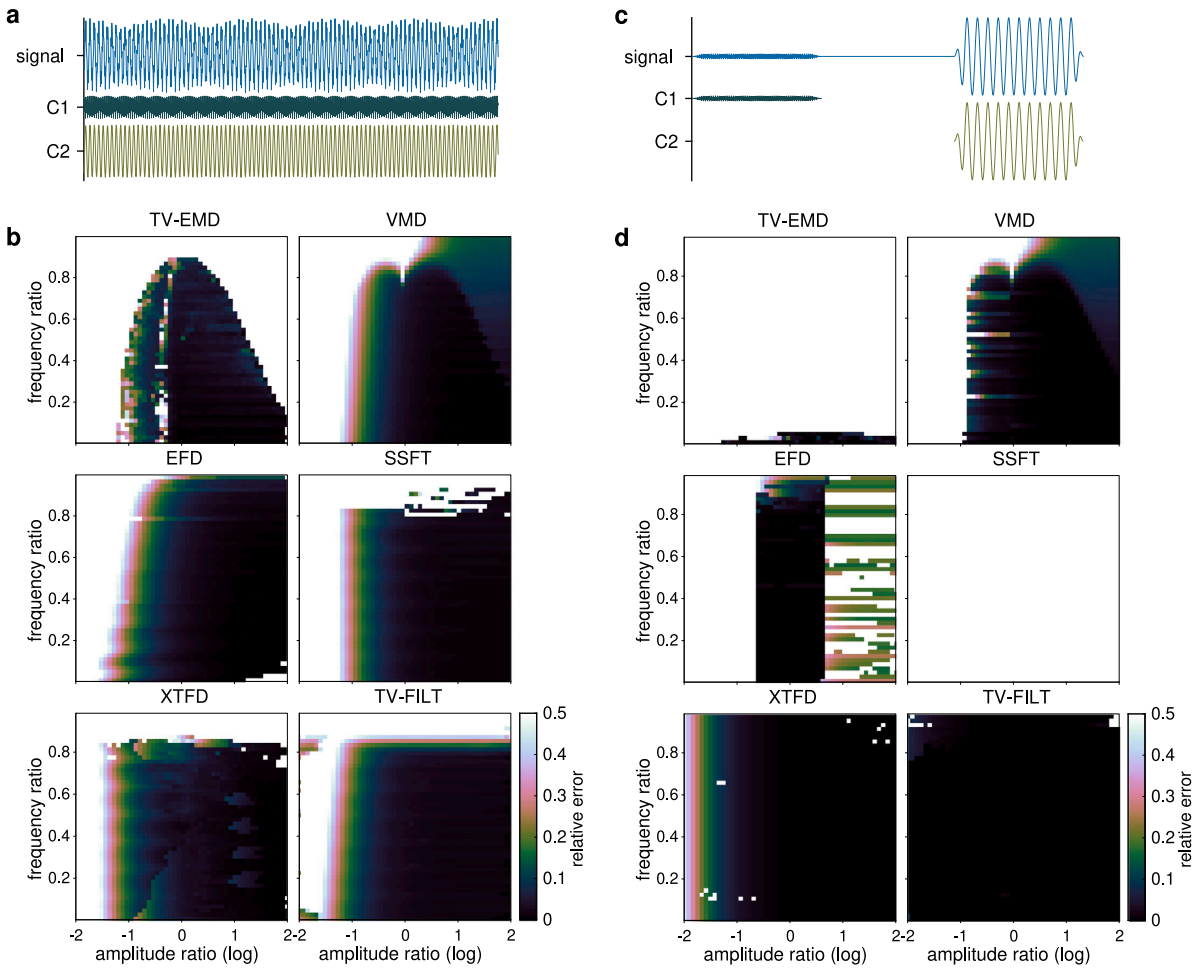


Fig. 3. Two two-tone tests using 6 different decomposition methods. Example signal with components C1 and C2 in (**a**) for the first test and example signal in (**c**) for the second test. For the first test, both components are present for the full duration of signal. Components are time-limited and separated in time for the second test. Frequency and amplitude of C2 is varied. Relative error is calculated for 6 decomposition methods for the estimate of the static tone and presented in (**b**) and (**d**). Amplitude- and frequency-ratios of C2 to C1 are $(2.3, 0.3)$ in (**a**) and $(15.3, 0.1)$ in (**b**). Abbreviations: TV-EMD, time-varying empirical decomposition mode; VMD, variational mode decomposition; EFD: empirical Fourier decomposition; SSFT: synchrosqueeze short-time Fourier transform; XTFD: cross time–frequency distribution; TV-FILT, time-varying filtering.

4. Results and discussion

Fig. 3 illustrates the results of the two-tone tests from Section 3.3. For the first test (Fig. 3a), signal decomposition performance for the proposed XTFD and TV-filtering methods across a range of amplitude and frequency ratios is as good as, or better than, other methods with low relative errors across a large range of amplitude and frequency ratios. All methods perform poorly at very low amplitude ratios (< 0.03) and high frequency ratios (> 0.8). The EFD has superior performance at high frequency ratios. The challenge for the XTFD and TV-filtering methods is in estimating the IF laws from the QTFD at low amplitude ratios or high frequency ratios. The proposed methods show superior performance in signal decomposition for time-limited components compared to all other methods (see Fig. 3b). Our decomposition methods provide near perfect reconstruction across all amplitude and frequency ratios. The TV-EMD and SSFT methods, in sharp contrast, fail to reconstruct the time-limited components because of inherent mode mixing across time in these techniques. Over a limited range of amplitude ratios, the VMD performs well.

When applied to a real world, nonstationary multi-component signal, the proposed methods extract components that align with our visual interpretation of individual components within the QTFD: Fig. 4 illustrates the proposed decompositions applied to a bat echolocation pulse. Individual components are well localized in the joint time–frequency domain and a composite QTFD constructed of QTFDs of individual components summed together shows close adherence to the QTFD of the original signal—see Fig. 4(a–c). This is not the case for other methods, such as the TV-EMD, EFD, and VN-CMD (see Fig. S1 in the Supplementary Material). The EFD is limited to the extraction of only stationary components (Fig. S1g); the VN-CMD extracts components with similar IF laws (Fig. S1j) while failing to represent the signal (large residual, Fig. S1l); and the TV-EMD extracts components with discontinuous IF laws (Fig. S1a). The SSFT provides an improved decomposition but is, nevertheless, corrupted by some mode mixing—components four and five (Fig. S1d and Fig. S1e) for instance—and fails to represent the complete signal (large residual, Fig. S1f). Note, we included the VN-CMD and not the VMD in this example as the VN-CMD was specifically proposed to address the limiting narrow band assumption of the VMD [15].

For a complex, simulated multi-component signal in the presence of noise, the residual of the XTFD more closely matches the noise component of the simulated signal, whereas the TV-filtering decomposition spreads the noise throughout the components: see Fig. 5. This is because the TV-filtering attempts to span the entire TF domain using wide filter bandwidths to ensure a zero residual. As the XTFD focuses on the local energy peak it is, therefore, more narrowband resulting in a more accurate representation of signal components in the presence of noise. Both methods, nevertheless, provide an accurate representation of the underlying signal components (see Table S2 in the Supplementary Material). This performance is preserved across increasing SNR and is

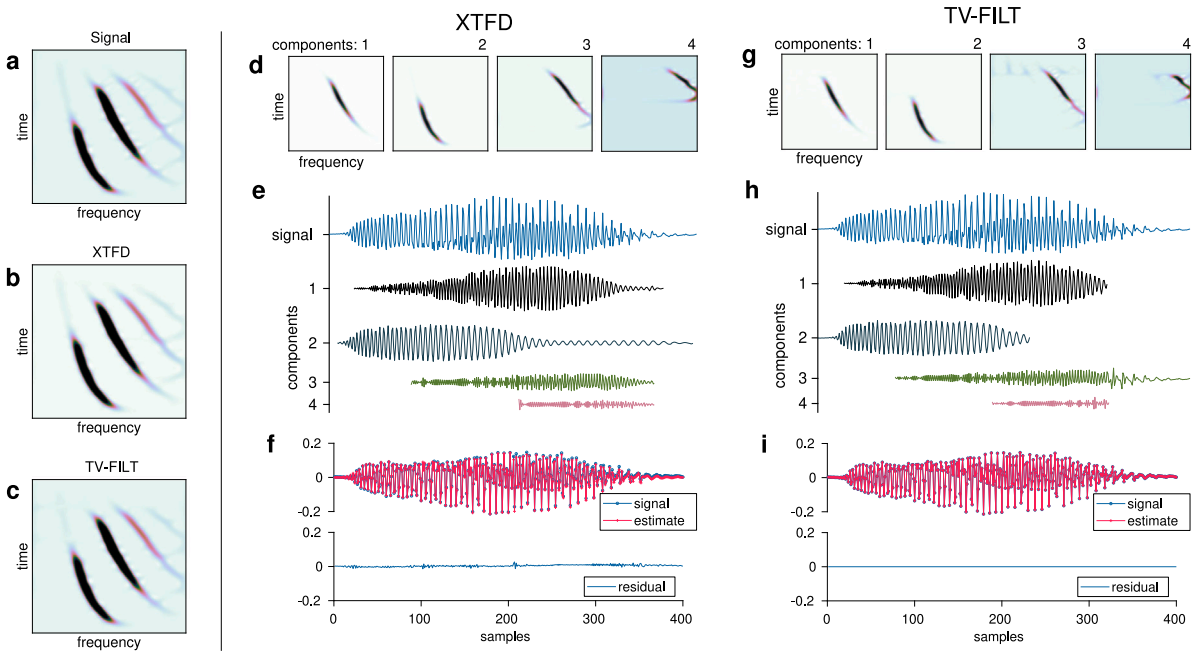


Fig. 4. Signal decomposition with the bat echolocation signal for the proposed methods. Time–frequency distribution (TFD) of the signal in (**a**) and TFDs for components extracted using the proposed cross-TFD (XTFD) and time-varying filtering (TV-FILT) methods in (**b**) and (**c**). A TFD is generated for each component and then combined in (**b**) and (**c**); for example, the TFD in (**b**) is the sum of the TFDs in (**d**). A maximum threshold (0.3 of normalized TFD energy) is applied to each of these TFD plots to enhance visualization of the components. TFD of individual components in (**d**) and (**g**) for both methods; signal with extracted components in (**e**) and (**h**); and difference (residual) between sum of components and signal in (**f**) and (**i**). Amplitude of components are plotted relative to signal amplitude in (**e**) and (**h**).

Table 1
Performance of nonstationary signal decomposition methods. Results are presented as $a/b(c)$ where a is the minimum number of components contributing at least 90% of the signal energy, b is the reconstruction accuracy (relative error) of sum of the a components, and c is the ratio of the number of stochastic to deterministic components (SDR). The number of stochastic components is averaged across both noise processes (white and fractional). Signals are two sinusoids (2-sin), a multi-component nonlinear signal (nonlinear), fractional and white Gaussian noise (noise), and a bat echolocation signal (bat).

	2-sin[a]	2-sin[b] (time-limited)	Bat	Nonlinear	Noise (white)	Noise (fractional)
TV filtering	2/0.0 (5.3)	2/0.0 (5.3)	2/0.09 (5.3)	3/0.0 (3.5)	11/0.04 (1)	10/0.04 (1.1)
cross-TFD	2/0.0 (6)	2/0.0 (6)	3/0.2 (4)	3/0.18 (4)	12/0.17 (1)	12/0.21 (1)
EFD[c]	99/0.0 (0.3)	74/0.03 (0.4)	68/0.45 (0.4)	62/0.88 (0.5)	24/0.8 (1.2)	32/1.05 (0.9)
TV-EMD	2/0.0 (3.8)	1/0.0 (7.5)	3/0.01 (2.5)	50/0.0 (0.5)	8/0.07 (0.9)	7/0.08 (1.1)
SSFT	2/0.0 (1.8)	1/0.0 (3.5)	2/0.09 (1.8)	3/0.05 (1.2)	4/0.07 (0.9)	3/0.21 (1.2)
VMD	2/0.0 (1)	2/0.0 (1)	2/0.0 (2.0)	1/0.0 (1)	2/0.0 (1)	2/0.4 (1)
VN-CMD	1/2.5 (2.5)	2/1.46 (1.3)	1/4.93 (2.5)	3/0.18 (0.8)	4/0.61 (0.6)	1/2.48 (2.5)

Key: TV, time varying; EFD, empirical Fourier transform; EMD, empirical mode decomposition; TFD, time–frequency distribution; VMD, variational mode decomposition; SSFT: synchrosqueeze short-time Fourier transform; VN-CMD, variational nonlinear chirp mode decomposition.

[a] Amplitude ratio of 0.91 and frequency ratio of 0.78.

[b] Amplitude ratio of 0.91 and frequency ratio of 0.19.

[c] Maximum number of components set to 100 for the EFD method.

maximal compared to other methods of decomposition, as illustrated in Fig. 6. The XTFD outperforms all other methods across a range of SNR, with the SSFT providing the best performance of existing methods (see Fig. 6).

The number of components extracted from our test signals for each of our decomposition methods is shown in Table 1. The majority of methods produce less components for deterministic compared to stochastic signals (SDR>1) with the exception of the EFD which, without *a priori* knowledge of the number of required components, tends to overdecompose deterministic nonstationary signals. Only our proposed methods (XTFD and TV filtering) return the correct number of components for both two-tone signals (Table 1). All methods have difficulty decomposing signals with wide support in both time and frequency domains such as stochastic noise, with the exception of the VN-CMD which does not decompose the signal at all. This is expected as stochastic signals will not have continuity in either the time or frequency domain resulting in many IF laws in the QTFD. Fig. 7 illustrates that the extracted components for the fractional Gaussian noise are compact both in time and frequency, in contrast to the TV-EMD for example (Fig. 7e) which does not separate components in time. (Examples with other methods are presented Fig. S2 in Supplementary Material.) This is a desirable aspect of decomposition and permits the use of component number as a surrogate measure of compactness to highlight differences between deterministic and stochastic signals. It is also noted that the TV filtering method produces slightly less components (10 vs. 12 and 11 vs. 12) than the XTFD when decomposing stochastic signals suggesting an XTFD measure of compactness may be more informative. This is due to the increased bandwidth of the time-varying filters compared to the XTFD permitting more accurate reconstruction of wide band signals such as noise. Nevertheless, both TV filtering and XTFD provide a more compact decomposition of nonstationary multi-component signals relative to wide band noise (see SDR in Table 1).

The computational efficiency of each method is evaluated across all test signals and is presented in Table 2. The processing required for

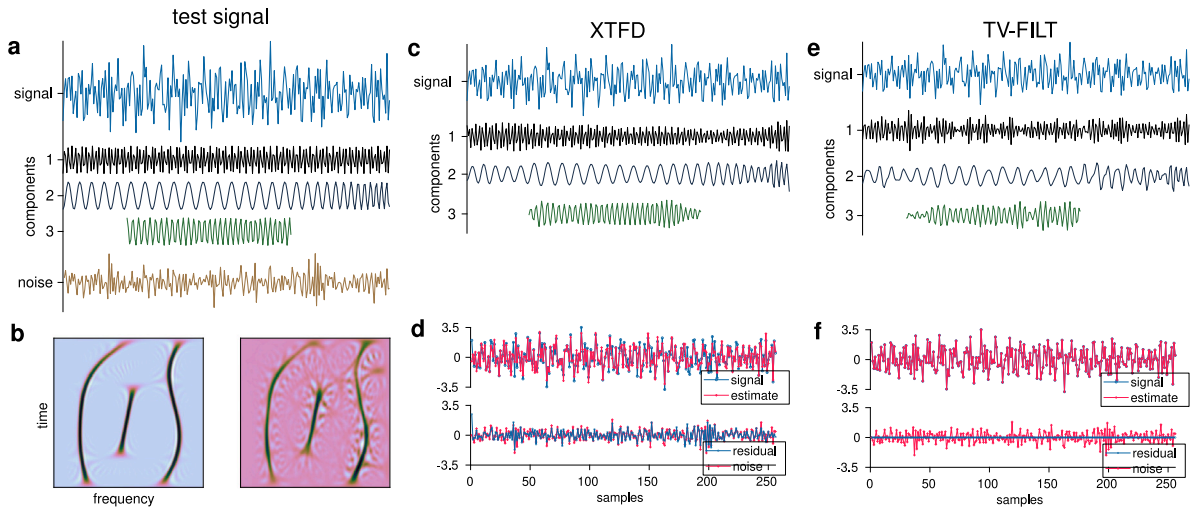


Fig. 5. Signal decomposition with a test signal consisting of 3 frequency-modulated components and fractional Gaussian noise. Time–frequency distributions (TFDs) in (**b**) of the test signal in (**a**) without (left) and with (right) noise. Methods: cross TFD (XTFD) in (**c**) and (**d**) and time-varying filtering (TV-FILT) in (**e**) and (**f**). Difference (residual) between sum of components and signal in (**d**) and (**f**). The noise component, at a signal-to-noise ratio of 5 dB, is also added to the these plots to illustrate the similarity between the residual and the noise for the XTFD method.

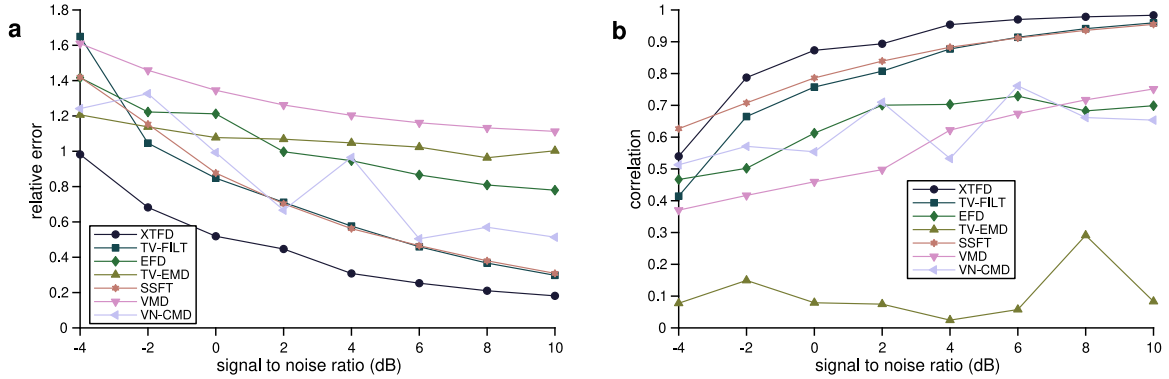


Fig. 6. Extracting the components of the multi-component nonlinear test signal presented in Fig. 5 from fractional Gaussian noise. Average relative error and average correlation of the 3 components against varying degrees of noise power. Comparing proposed methods (XTFD and TV-FILT) against existing approaches. Abbreviations: TV-EMD, time-varying empirical decomposition mode; VMD, variational mode decomposition; EFD: empirical Fourier decomposition; SSFT: synchrosqueeze short-time Fourier transform; XTFD: cross time–frequency distribution; TV-FILT, time-varying filtering.

the proposed methods includes estimating the time–frequency distributions (QTFDs and XTFDs), detecting IF laws through peak-tracking algorithms, and time-varying filtering for each component. Efficient algorithms are used to compute the QTFD and oversampled QTFD [30]. Computational speed for our methods fall within the range of the others methods, with the EFD as the fastest method across all signal types. For the two-tone signals, the XTFD is closer to the VMD in terms of computational speed (the slowest method for these signals) because the TFD generated for this signal is over-sampled in the frequency direction by a factor of 8 (see Table S1 in Supplementary Material).

Our methods outperform stationary methods (EDF), sifting-based methods (TV-EMD), optimization methods (VMD and VN-CMD), and time–frequency methods (SSFT) in terms of accuracy and compactness, particularly for signals whose components are disjoint in the time–frequency domain. Stationary methods are hampered by variable frequency content that spans a large frequency range. Methods based on sifting are limited by variable frequency content that cross the natural frequency-based division of the sifting process [10], components that are separated in time, and the presence of noise in the signal. The VMD is limited by the requirement for bandwidth optimization of each component and *a priori* estimates of component centre frequency which may be difficult to estimate.

The superior performance of our methods is linked to the specific signal class we have analysed in this research. We have tried to incorporate a broad class of signals but it is certainly not complete. Therefore, the relative performance of our methods on a different class of signals may differ. For example, sifting-based methods perform intuitively for non-sinusoidal waveforms (e.g. Stokes waves) by combining harmonics into a single IMF. Although this makes sense from a physical perspective, it may not always be the most useful representation for a signal analyst. The bat echolocation pulse is an excellent counter-example as harmonics have different support in time (see Fig. 4) which are better captured by our decomposition methods (and, to a lesser degree, the SSFT—see Fig. S1 in the Supplementary Material).

While our work is primarily focused on methods of converting regions of a QTFD, identified through IF laws, into time-domain signal components, the earlier stages of the decomposition process, namely the QTFD and IF estimation are critical to this process. We expect that multi-component signals with wide band transients and components that intersect in the time–frequency domain will be difficult to decompose with our method. Alternatives to our simple peak-tracking algorithm [25] may help overcome some of these limitations (for example see [27]). Also, the smoothing applied when formulating the QTFD can greatly affect its ability to resolve energy in the time–frequency plane and therefore estimation of the IF laws. The extraction of the IF

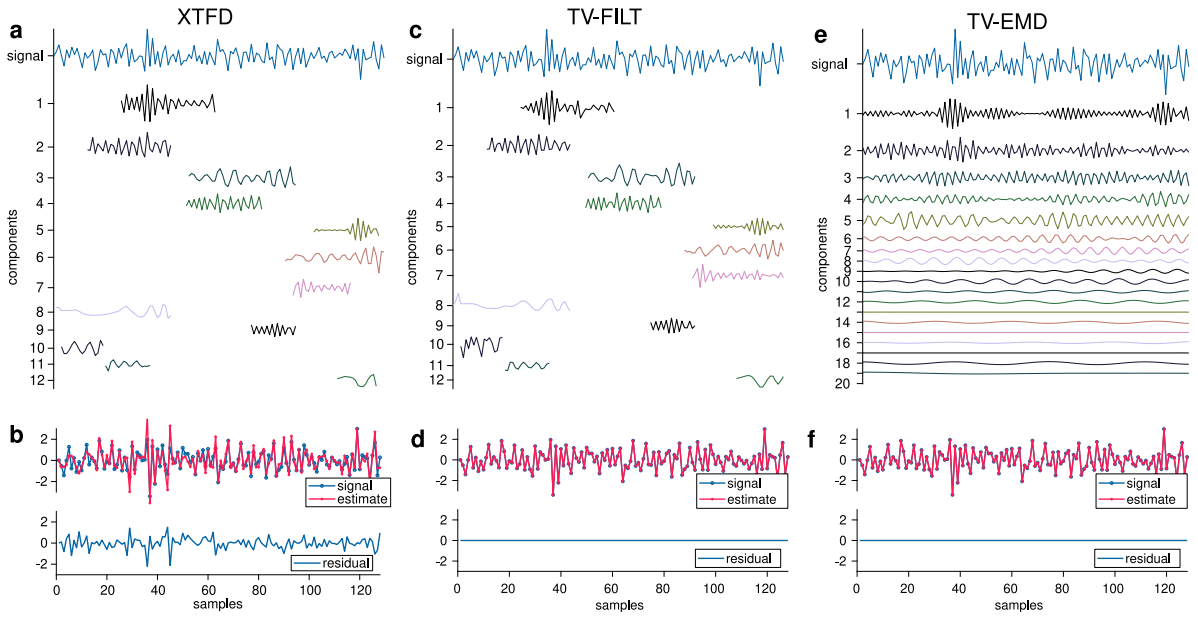


Fig. 7. Signal decomposition with fractional Gaussian noise, comparing proposed methods (XTFD and TV-FILT) with existing method (TV-EMD). Left: cross time–frequency distribution (XTFD) in (**a**) and (**b**); middle: time-varying filtering (TV-FILT) in (**c**) and (**d**); and right: time-varying empirical mode decomposition (TV-EMD) in (**e**) and (**f**). Signal with components in (**a**), (**c**), and (**e**). Difference (residual) between sum of components and signal in (**b**), (**d**), and (**f**). Amplitude of components are plotted relative to signal amplitude for (**a**), (**c**), and (**e**).

Table 2
Computation time in milliseconds for a range of decomposition methods and test signals presented as mean (standard deviation) over 100 iterations. Empirical Fourier transform (EFD) is the fastest method for all signals; slowest method per signal is highlighted in bold. Signals are two sinusoids (2-sin), a multi-component nonlinear signal (nonlinear), fractional Gaussian noise (noise), and a bat echolocation signal (bat).

	2-sin	2-sin (time-limited)	Nonlinear	Noise	Bat
TV filtering	220 (26)	177 (13)	65 (17)	20 (2)	62 (13)
cross-TFD	1416 (131)	1200 (95)	40 (4)	14 (<1)	48 (3)
EFD	13 (3)	12 (<1)	2 (<1)	1 (<1)	3 (<1)
TV-EMD	655 (77)	111 (8)	**8253 (105)**	**711 (17)**	**1087 (22)**
SSFT	407 (58)	197 (7)	71 (3)	38 (2)	105 (5)
VMD	**1462 (195)**	**1211 (16)**	199 (4)	106 (3)	328 (12)
VN-CMD	1352 (162)	1091 (236)	337 (17)	279 (4)	743 (15)

Key: TV, time varying; EFD, empirical Fourier transform; EMD, empirical mode decomposition; TFD, time–frequency distribution; VMD, variational mode decomposition; SSFT: synchrosqueeze short-time Fourier transform; VN-CMD, variational nonlinear chirp mode decomposition.

laws goes to the heart of how signal components are defined and how information is shared between $\theta_j[n]$ and $a_j[n]$ in (10) of which there are an infinite number of combinations that can generate the same signal component. We have attempted to select a set of default parameters based on heuristics defining the energy and span of signal components to ensure that no spurious signal components are output while preserving our general intuition of signal decomposition, i.e. component numbers for deterministic signals should be considerably less than for stochastic signals. However, some manipulation of these parameters may alter the decomposition.

In conclusion, we present two new methods for decomposing nonstationary multi-component signals. By defining a decomposition directly from a joint representation of time–frequency energy, we extract regions of localized energy that reflect the visual interpretation of components in a QTFD. We show that for the selected signals our methods show improved performance over several methods for accurately representing signal components, particularly for signals with time-limited components. The key outstanding question is whether the application of these methods improves the accessibility of important information within a signal, particularly for tasks where nonstationarity confounds traditional methods.

CRediT authorship contribution statement

J.M. O'Toole: Writing – review & editing, Writing – original draft, Visualization, Validation, Software, Methodology, Investigation, Formal analysis, Data curation, Conceptualization. **N.J. Stevenson:** Writing – review & editing, Validation, Software, Methodology, Investigation, Formal analysis, Data curation, Conceptualization.

Acknowledgements

JOT was supported by Science Foundation Ireland (15/SIRG/3580).

Appendix A. Supplementary data

Supplementary material related to this article can be found online at https://doi.org/10.1016/j.sigpro.2025.110095.

Data availability

Code is available at https://github.com/otoolej/tfd_decomp/.

References

[1] M.J. Fadili, J.L. Starck, J. Bobin, Y. Moudden, Image decomposition and separation using sparse representations: An overview, Proc. IEEE 98 (6) (2009) 983–994.

[2] R. Sharma, L. Vignolo, G Schlotthauer, M.A. Colominas, H.L. Rufiner, S.R. Prasanna, Empirical mode decomposition for adaptive AM-FM analysis of speech: A review, Speech Commun. 88 (2017) 39–64.

[3] A.R. Lindsey, Wavelet packet modulation for orthogonally multiplexed communication, IEEE Trans. Signal Process. 45 (5) (1997) 1336–1339.

[4] M. Ashoori, J.M. O'Toole, K.D. O'Halloran, G. Naulaers, L. Thewissen, J. Miletin, P.Y. Cheung, A. EL-Khuffash, D. Van Laere, Z. Straňák, et al., Machine learning detects intraventricular haemorrhage in extremely preterm infants, Children 10 (6) (2023) 917.

[5] A.M. Gaouda, M.M. Salama, M.R. Sultan, A.Y. Chikhani, Power quality detection and classification using wavelet-multiresolution signal decomposition, IEEE Trans. Power Deliv. 14 (4) (1999) 1469–1476.

[6] S. Mallat, A Wavelet Tour of Signal Processing, Academic Press, London, UK, 1998.

[7] A.V. Oppenheim, R.W. Schafer, Discrete-Time Signal Processing, Prentice-Hall, New Jersey, USA, 1999.

[8] S.S. Chen, D.L. Donoho, M.A. Saunders, Atomic Decomposition by Basis Pursuit, SIAM Rev. 43 (1) (2001) 129–159.

[9] N.E. Huang, Z. Shen, S.R. Long, M.C. Wu, H.H. Shih, Q. Zheng, N.C. Yen, C.C. Tung, H.H. Liu, The empirical mode decomposition and the Hilbert spectrum for nonlinear and non-stationary time series analysis, Proc. R. Soc. Lond. A 454 (1) (1998) 903–995.

[10] P. Flandrin, G. Rilling, P. Gonçalvés, Empirical mode decomposition as a filter bank, IEEE Signal Process. Lett. 11 (2) (2004) 112–114.

[11] Z. Wu, N.E. Huang, Ensemble empirical mode decomposition: a noise-assisted data analysis method, Adv. Adapt. Data Anal. 01 (01) (2009) 1–41.

[12] K. Dragomiretskiy, D. Zosso, Variational mode decomposition, IEEE Trans. Signal Process. 62 (3) (2014) 531–544.

[13] H. Li, Z. Li, W. Mo, A time varying filter approach for empirical mode decomposition, Signal Process. 138 (2017) 146–158.

[14] M. Jabloun, Ordinal pattern-based mode decomposition: A new approach to time series analysis, Signal Process. 230 (2025) 109802.

[15] S. Chen, X. Dong, Z. Peng, W. Zhang, G. Meng, Nonlinear chirp mode decomposition: A variational method, IEEE Trans. Signal Process. 65 (22) (2017) 6024–6037.

[16] X. Tu, J. Swärd, A. Jakobsson, F. Li, Estimating nonlinear chirp modes exploiting sparsity, Signal Process. 183 (2021) 107952.

[17] I. Daubechies, J. Lu, H.T. Wu, Synchrosqueezed wavelet transforms: An empirical mode decomposition-like tool, Appl. Comput. Harmon. Anal. 30 (2) (2011) 243–261.

[18] I. Daubechies, S. Maes, A nonlinear squeezing of the continuous wavelet transform based on auditory nerve models, in: Wavelets in Medicine and Biology, Routledge, 2017, pp. 527–546.

[19] L. Li, H. Cai, H. Han, Q. Jiang, H. Ji, Adaptive short-time Fourier transform and synchrosqueezing transform for non-stationary signal separation, Signal Process. 166 (2020) 107231.

[20] L. Cohen, Time–frequency distributions—a review, Proc. IEEE 77 (7) (1989) 941–981.

[21] L. Cohen, Time–frequency Analysis, Prentice-Hall PTR, New Jersey, USA, 1995.

[22] B. Boashash (Ed.), Time–Frequency Signal Analysis and Processing: A Comprehensive Reference, Elsevier, Oxford, UK, 2003.

[23] Z. Yang, L. Yang, C. Qing, D. Huang, A method to eliminate riding waves appearing in the empirical AM/FM demodulation, Digit. Signal Process. 18 (4) (2008) 488–504.

[24] J.M. O'Toole, M. Mesbah, B. Boashash, Improved discrete definition of quadratic time–frequency distributions, IEEE Trans. Signal Process. 58 (2) (2010) 906–911.

[25] R.J. McAulay, T.F. Quatieri, Speech analysis/synthesis based on a sinusoidal representation, IEEE Trans. Acoust. Speech Signal Process. 34 (4) (1986) 744–754.

[26] D. Iatsenko, P.V.E. McClintock, A. Stefanovska, Nonlinear mode decomposition: A noise-robust, adaptive decomposition method, Phys. Rev. E 92 (3) (2015) 032916, ISSN: 1550–2376.

[27] S. Chen, X. Dong, G. Xing, Z. Peng, W. Zhang, G. Meng, Separation of overlapped non-stationary signals by ridge path regrouping and intrinsic chirp component decomposition, IEEE Sens. J. 17 (18) (2017) 5994–6005.

[28] N.J. Stevenson, J.M. O'Toole, L.J. Rankine, G.B. Boylan, B. Boashash, A non-parametric feature for neonatal EEG seizure detection based on a representation of pseudo-periodicity, Med. Eng. Phys. 34 (4) (2012) 437–446.

[29] E. Bedrosian, A product theorem for Hilbert transforms, Proc. IEEE 51 (1963) 868–869.

[30] J.M. O'Toole, B. Boashash, Fast and memory-efficient algorithms for computing quadratic time–frequency distributions, Appl. Comput. Harmon. Anal. 35 (2) (2013) 350–358.

[31] G. Wang, The most general time-varying filter bank and time-varying lapped transforms, IEEE Trans. Signal Process. 54 (10) (2006) 3775–3789.

[32] G. Rilling, P. Flandrin, One or two frequencies? The empirical mode decomposition answers, IEEE Trans. Signal Process. 56 (1) (2008) 85–95.

[33] W. Zhou, Z. Feng, Y.F. Xu, X. Wang, H. Lv, Empirical Fourier decomposition: An accurate signal decomposition method for nonlinear and non-stationary time series analysis, Mech. Sys. Signal Process. 163 (2022) 108155.

[34] J.M. O'Toole, B. Boashash, Time-frequency detection of slowly varying periodic signals with harmonics: Methods and performance evaluation, EURASIP J. Adv. Signal Process. 2011 (2011) 193797.

[35] G. Thakur, H.T. Wu, Synchrosqueezing-based recovery of instantaneous frequency from nonuniform samples, SIAM J. Math. Anal. 43 (5) (2011) 2078–2095.